JACS
JOURNAL OF THE AMERICAN CHEMICAL SOCIETY

ARTICLE

pubs.acs.org/JACS

Boron Carbon Nitride Nanostructures from Salt Melts: Tunable Water-Soluble Phosphors

Weiwei Lei,[†] David Portehault,*[,†,§] Rumiana Dimova,[‡] and Markus Antonietti[†]

[†]Department of Colloid Chemistry, and [‡]Department of Theory and Bio-Systems, Max-Planck-Institute of Colloids and Interfaces, Research Campus Golm, 14424 Potsdam, Germany

[§]UPMC Univ Paris 06, CNRS, UMR 7574, Chimie de la Matière Condensée de Paris, Collège de France, 11 place Marcelin Berthelot, 75231 Paris Cedex 05, France

Supporting Information

ABSTRACT: A simple, high yield, chemical process is developed to fabricate layered *h*-BN nanosheets and BCNO nanoparticles with a diameter of ca. 5 nm at 700 °C. The use of the eutectic LiCl/KCl salt melt medium enhances the kinetics of the reaction between sodium borohydride and urea or guanidine as well as the dispersion of the nanoparticles in water. The carbon content can be tuned from 0 to 50 mol % by adjusting the reactant ratio, thus providing precise control of the light emission of the particles in the range 440−528 nm while reaching a quantum yield of 26%. Because of their green synthesis, low toxicity, small size, and stability against aggregation in water, the as-obtained photoluminescent BCNO nanoparticles show promise for diagnostics and optoelectronics.

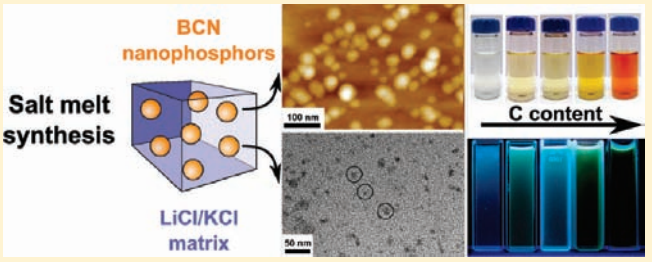

1. INTRODUCTION

Graphene was recently put on the foreground of material science. Among its exciting properties, one can distinguish quantum transport and mechanical properties strongly differing from graphite, the "stacked form" of graphene.[1,2] Structurally similar to graphite but different from the property point of view is hexagonal boron nitride (*h*-BN), a wide band gap semiconductor with high resistance to corrosion, high thermal conductivity, and strong UV-emission.[3,4] It is industrially implemented as high performance lubricant as well as for optoelectronic devices. As an analogue to graphene, single layer *h*-BN is now urgently sought for first to complement models based on graphene for heat and electron transport in 2D structures, and second to discover novel behavior, which cannot be observed in the highly conductive graphene.[5,6] More generally, controlling the shape and size of *h*-BN related nanostructures could pave the way to innovative and intriguing materials.[7,8] In addition, doping of graphene, especially with light elements such as boron and nitrogen, is now believed to provide an additional way to tune transport properties,[9−12] but it is still a challenge while keeping an exquisite control of carbon nanostructures. On the opposite side of the B−C−N ternary phase diagram, adjustment of the carbon composition within layered BN compounds seems to be more developed where recent advances performed by our group and others have shown that control of the carbon and the oxygen content in (B,N) rich boron carbon nitride (BCN) nanostructures modifies considerably the H_2 sorption and the light emission properties.[8,13,14] Especially, theoretical calculations[15,16] followed by experimental evidence[13,14,17,18] have indicated that visible light emission with tunable wavelength can be achieved in BCNO compounds, which can then be considered as metal-free phosphors with low toxicity.

Although many synthetic procedures have been proposed for the synthesis of BCN nanostructures,[19−27] chemical processes seem to be the most suitable means to tune their composition and morphology considering simplicity and versatility.[8,13,14,23,27] Particularly, chemical syntheses enable one to envision nanostructures readily dispersible in suitable solvents, a requirement for biomedical applications based on aqueous systems. The few related protocols that were recently proposed are based on templating approaches, which hinder dispersion or require elaborated post-treatments and size selection to achieve dispersion.[8,13,14,23,27] An innovative synthesis approach in this field should therefore provide easy access to B(C)N(O) nanostructures with high yield, controlled composition, morphology, dispersion, and emission properties.

In this study, we report the facile synthesis of BN and BCNO compounds in a simple eutectic salt melt. This environmentally friendly solution route yields B(C)N(O) with adjustable carbon and oxygen contents, as well as nanostructure control ranging from nanosheets to 5 nm nanoparticles. These materials do not contain any heavy metal and are believed to be environmentally

Received: January 27, 2011
Revised: March 29, 2011
Published: April 20, 2011

benign with a low toxicity. Particles are readily dispersed in water and exhibit photoluminescence, which is governed by the elemental composition.

2. EXPERIMENTAL SECTION

Synthesis of Colloidal Nanosheets and Nanoparticles. Sodium borohydride was used as boron precursor, and urea (CH_4N_2O) or guanidine hydrochloride (CH_5N_3,HCl) was chosen as carbon and nitrogen sources with varying N content. The eutectic mixture LiCl/KCl (45/55 wt) was selected as a cheap, environmentally friendly, water-soluble, high temperature solvent with comparably low melting point (355 °C). LiCl and KCl (Aldrich) were previously mixed and finely ground in a mortar. The resulting mixture LiCl/KCl was evacuated at 200 °C for 4 days. Next, the solvent LiCl/KCl was transferred into an argon-filled glovebox. The sodium borohydride (2 mmol) and the C/N molecular source in adequate amounts were added into the eutectic mixture LiCl/KCl (2.5 g), and then the powder mixtures were ground finely with a Retsch MM400 ballmill (airtight vials of 50 mL, one steel ball of 62.3 g, and a diameter of 23 mm) for 2 min at 60 Hz. The resulting powder was heated to 700 °C at a rate of 5 °C min^{-1} for 2 h under nitrogen flow. After being cooled to room temperature, the obtained powders from white to brown were dissolved in water. The resulting B(C)N(O) aqueous dispersion was dialyzed for 1 week (membrane cutoff: 3500 kDa) in pure water to remove the salts. Stable aqueous dispersions were then obtained. The C/O content can be easily tuned by changing the C/N source and the ratio of sodium borohydride versus urea or guanidine hydrochloride. In this Article, the specimens are labeled according to the starting materials and their molar ratio: sodium borohydride/urea = 1/1, 1/10 for **BU-11** and **BU-110**, sodium borohydride/guanidine hydrochloride = 1/1, 1/5, 1/10, 1/15 for **BG-11**, **BG-15**, **BG-110**, and **BG-115**, respectively. After drying of the dispersions, typical syntheses of **BU-11** and **BG-110** based on 2.5 g of eutectic solvent and 2 mmol of sodium borohydride yield, respectively, 200 and 150 mg of nanopowders.

Characterization. X-ray diffraction (XRD) measurements were performed on a D8 Bruker apparatus operating at the Cu $K_{\alpha 1}$ radiation. Scanning electron microscopy (SEM) was performed on a LEO 1550-Gemini instrument. The samples were loaded on carbon-coated stubs and coated by sputtering an Au/Pd alloy prior to imaging. Electron microscopy (TEM) was performed on a Technai 120 (operating at 120 kV) apparatus. Samples were prepared by evaporating a drop of diluted suspension in ethanol on a carbon-coated copper grid. HRTEM studies were carried out by using a JEOL JEM 2011 LaB_6 (operating at 200 kV) apparatus at the Centre for Microscopy, UPMC, Paris. The atomic force microscopy (AFM) measurements were performed on a Veeco instrument. Before observation, the samples dispersed in water were dropped on a mica substrate. X-ray spectroscopy (XPS) was performed at the Service of Nanotechnology and Surface analysis (C.A.C.T.I.) of Vigo University. Analysis of the samples was performed using a Thermo Scientific K-Alpha ESCA instrument equipped with aluminum $K_{\alpha 1,2}$ monochromatized radiation at 1486.6 eV X-ray source. Because of the nonconducting nature of the samples, it was necessary to use an electron flood gun to minimize surface charging. Neutralization of the surface charge was performed by using both a low energy flood gun (electrons in the range 0−14 eV) and a low energy argon ions gun. The XPS measurements were carried out using monochromatic Al K radiation ($h\nu$ = 1486.6 eV). Photoelectrons were collected from a take-off angle of 90° relative to the sample surface. The measurement was done in a Constant Analyzer Energy mode (CAE) with a 100 eV pass energy for survey spectra and 20 eV pass energy for high resolution spectra. Charge referencing was done by setting the lower binding energy C1s photo peak at 285.0 eV C1s hydrocarbon peak.[28] Surface elemental composition was determined using the standard Scofield photoemission cross sections. The zeta potential of the nanoparticles dispersed in water was measured by using a Zetasizer Nano ZS90 apparatus from Malvern operating at 633 nm and equipped with a Multi Purpose Titrator MPT2, which was filled with a 2 mol L^{-1} HNO_3 solution used to adjust the pH of the colloidal dispersion. The dynamic light scattering (DLS) measurements were performed on the aqueous dispersions of BCNO nanoparticles with a Zetasizer Nano ZS Zen3500 at 25 °C. The UV−visible absorption spectra were obtained with a Lambda 2 spectrometer. The emission spectra were recorded on a Fluoromax-4 spectrometer (Horiba Jobin Yvon Inc.). The quantum yield (QY) was determined by comparison with ethanol solution of rhodamine B (quantum yield: 70%).[14] For confocal imaging, giant unilamellar vesicles were prepared via the method of electroformation.[29] The vesicles were made of dioleoylphosphatidylcholine (DOPC) and a small fraction (0.1 mol %) of the fluorescent dye 1,1′-dioctadecyl-3,3,3′,3′-tetramethylindocarbocyanine perchlorate ($DiIC_{18}$). DOPC was purchased from Avanti Polar Lipids Inc. (Alabaster, AL), and $DiIC_{18}$ was obtained from Molecular Probes (Leiden, The Netherlands; excitation wavelength at 551 nm and emission wavelength at 569 nm). The vesicles were grown in 100 mmol L^{-1} sucrose solution and subsequently diluted in isoosmolar glucose solution. Apart from ensuring better phase contrast of the microscopy images, this step allows settling of the vesicles to the bottom of the observation chamber and thus easy location and imaging. The osmolarities of the sucrose and glucose solutions were measured with the cryoscopic osmometer Osmomat 030 (Gonotec, Berlin, Germany). After preparation, the vesicle solution was mixed with a solution of the **BG-15** sample in a 2:1 volume ratio. Fluorescence microscopy snapshots were acquired with a confocal laser scanning microscope Leica DM IRE2 (Leica Microsystems Heidelberg GmbH, Germany) using 40× Ph2 objective and laser excitation at 458 nm (Ar laser). Emission light was detected by a photomultiplier tube in the spectral ranges 470−550 nm (for the QDs) and 560−690 nm (for DiIC18). The measurements were performed at room temperature.

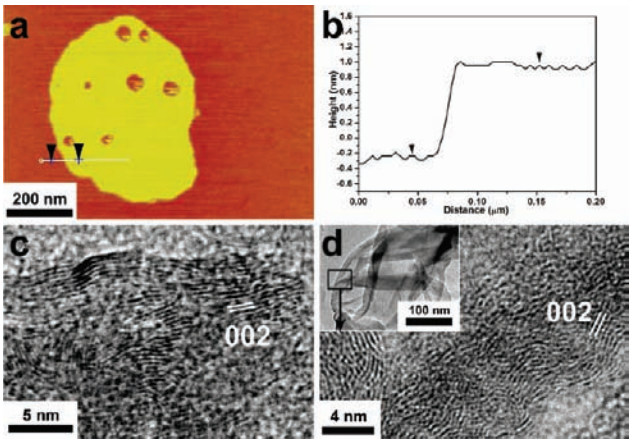

Figure 1. AFM picture (a) and corresponding line-scan profile (b) of **BU-11** sample. HRTEM and TEM (inset in (d)) pictures of **BU-11** (c) and **BG-11** (d).

3. RESULTS AND DISCUSSION

B(C)N(O) nanostructures were obtained by the reaction between harmless reagents sodium borohydride and urea or guanidine, at atmospheric pressure, in a molten eutectic mixture of LiCl and KCl as an environmentally friendly solvent. The nanostructures of the different samples were investigated by TEM and AFM. Panel a of Figure 1 shows a typical AFM image of **BU-11**, obtained with $NaBH_4$:urea = 1:1, which exhibits a sheet-like

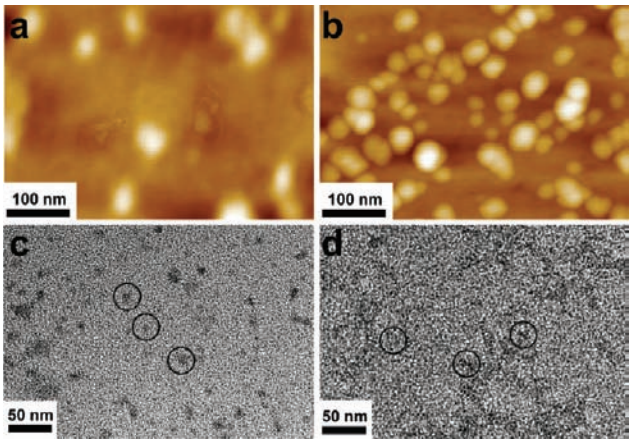

Figure 2. AFM (a,b) and TEM (c,d) pictures of **BU-110** (a,c) and **BG-115** (b,d) samples. Circles highlight some nanoparticles in the TEM pictures.

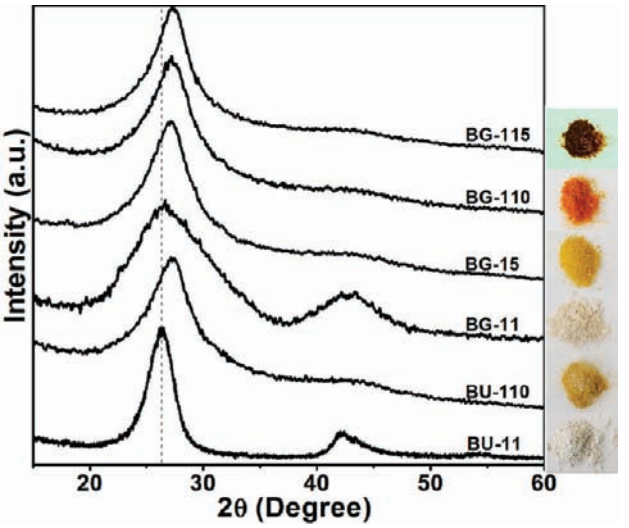

Figure 3. XRD patterns of **BU-11**, **BU-110**, and **BG-11** to **BG-115** samples. The insets are optical pictures of the corresponding dried powders.

nanostructure typical of layered turbostratic boron nitride. Some holes are frequently observed into the sheets, presumably due to uncomplete particle growth during the synthesis. The corresponding line-scan profile in Figure 1b indicates a thickness of about 1.2 nm, which corresponds to few *h*-BN layers.[5] Similar results are observed for the **BG-11** sample, obtained with $NaBH_4$: guanidine = 1:1. Figure 1c and d shows HRTEM images of edge regions of **BU-11** and **BG-11**. These folded back areas highlight the interlayer (002) lattice fringes (0.34 nm) of layered BN and suggest that samples obtained with a low amount of C/N sources are strongly related to *h*-BN and are made of nanosheets with 2−10 stacked BN layers.

The AFM and TEM pictures (Figure 2) of **BU-110** ($NaBH_4$: urea = 1:10) and **BG-115** ($NaBH_4$:guanidine = 1:15) show that both samples are composed of ca. 5 nm nanoparticles. AFM and TEM for the other samples (**BG-15** and **BG-110**, Supporting Information) confirm that all of the compounds obtained from high content of C/N source are made of 5 nm nanoparticles. The absence of lattice fringes from HRTEM and the strong broadening of the XRD peaks (Figure 3) suggest that the particles exhibit poor crystallinity or that the lattice is severely strained.

Figure 3 shows XRD patterns of a sequence of the dried samples **BU-11** to **BG-115**. A single hexagonal phase of BN is observed for **BU-11** and **BG-11**, with typical white powders highlighting the presence of a wide band gap semiconductor. The color of the other samples is red-shifted when the amount of C/N source is increased. XRD patterns typical of a turbostratic structure are then obtained. All samples show characteristic peaks centered at about 26° (2θ), belonging to the (002) interlayer reflection of *h*-BN. This peak is clearly shifted toward higher angles when moving from **BU-11** to **BG-115**, indicating a decrease of the interlayer spacing from 0.339 to 0.327 nm with increasing C doping level. The strong broadening of the peaks for every sample indicates the formation of nanosized samples and/or low correlation lengths. The Scherrer formula applied to the (002) reflection of **BU-11** yields a crystallite thickness of 2.5 nm, in agreement with HRTEM data. Samples **BU-110** and **BG-11** to **BG-115** exhibit a smaller correlation length along the (001)* direction, with ca. 1.9 nm, in agreement with the nanoparticle size and the poorly ordered structure.

To further investigate the local structure of the as-obtained materials, the chemical states of B, C, and N elements were investigated using XPS spectra. Figure 4a and b shows typical B1s and N1s spectra, respectively, for **BU-11**. The binding energy of B1s is 191.1 eV, while the N1s signal is at 398.6 eV. These values are very close to the previously reported values of few layers boron nitride with BN_3 and NB_3 trigonal units.[6,22] The shoulder at 192.5 eV in the B1s spectrum is assigned to the structure terminating B−O bonds. The XPS survey yields an elemental formula of $B_{1.0}C_{0.1}N_{0.9}O_{0.2}$, close to hexagonal BN. Noteworthy, only negligible amounts of oxygen are present, which underlines inertness toward oxidation upon air and water exposure. This is related to the good crystallinity of the nanosheets, as compared to other materials synthesized at similar temperatures (700−1000 °C), which are more disordered and very sensitive to oxidation.[8] High crystallinity *h*-BN usually requires much higher temperatures (T > 1000 °C) and/or high pressures to be obtained.[8,30] The different behavior in the present study may be ascribed to the beneficial effect of the liquid medium, which enhances reaction kinetics.[31] Figures 4c−e shows the XPS spectra of B1s, C1s, and N1s core level electrons for **BG-11** and **BG-15** (the XPS spectra of the other samples **BU-110**, **BG-110**, and **BG-115** are shown in the Supporting Information). The corresponding compositions were estimated from the XPS wide scan spectra: $B_{1.0}C_{6.8}N_{5.1}O_{1.7}$ (**BU-110**), $B_{1.0}C_{1.3}N_{1.2}O_{0.7}$ (**BG-11**), $B_{1.0}C_{7.5}N_{6.0}O_{1.6}$ (**BG-15**), $B_{1.0}C_{7.8}N_{6.0}O_{1.5}$ (**BG-110**), and $B_{1.0}C_{12}N_{9.5}O_{2.0}$ (**BG-115**). As expected, an excess of C/N precursors leads to higher N/B and C/B ratios as exemplified by **BG** samples. Guanidine acts as a better N donor, presumably because of its initial higher N content. Interestingly, the O/B ratio increases with an increase of the guanidine ratio. Because the particle size is similar for **BG-15**, **BG-110**, and **BG-115**, the increasing O/B ratio cannot account only for water and air sorption, but is more likely related to structural oxygen, presumably at the particle surface. The sensitivity of boron carbon nitrides to oxidation in contact with air and/or water is well documented,[8] and most probably leads to reaction between air and water to yield oxidized boron carbon nitrides after post-synthesis washing. An increase of the initial guanidine amount leads to higher content of carbon, which disturbs the boron environment within the covalent framework and could explain the

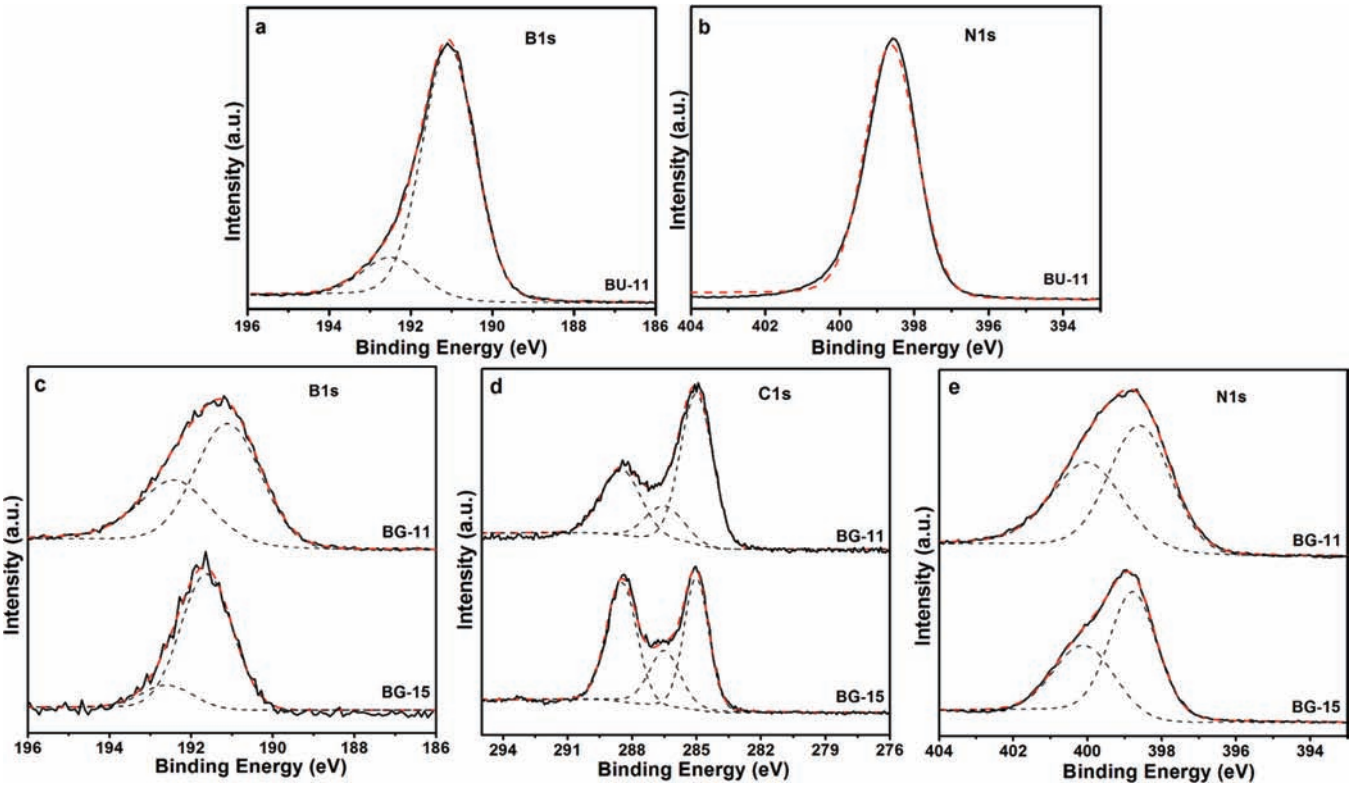

Figure 4. XPS spectra of **BU-11**, (a) B1s, (b) N1s, and **BG-11** and **BG-15** samples, (c) B1s, (d) C1s, (e) N1s.

increasing sensitivity to oxidation. The B1s spectra of **BG-11** and **BG-15** shown in Figure 4c can be fitted by Gaussian curves with dominating components centered at 191.1 and 191.6 eV, accompanied by small components peaked at 192.4 and 192.6 eV, respectively. The dominant peaks at low binding energies are attributable to typical layered BN as for **BU-11**, while the higher energy components are assigned to B−O bonds, thus confirming that boron atoms are the oxidation sensitive sites. No C−B or B−B signals are observed. The C1s spectra were fitted with three components at 285.0, 286.5, and 288.5 eV, corresponding respectively to C−C (284.7−285.5 eV),[26,27] C═N or C≡N (286.2−286.9 eV), and C−N (288.2−288.5 eV) bonds.[26,27,32] In the N1s spectra, the peak at 398.6 eV is assigned to N−B bonds.[26,27] The shoulder at higher energy accounts for the formation of C−N or C≡N bonds (approximately 400 eV).[26,27]

The FTIR spectra of **BU-11**, **BU-110**, and **BG-11** to **BG-115** with various contents of carbon are shown in Figure 5. For **BU-11**, two strong bands at 772 and 1398 cm^{-1} are assigned to the in-plane stretching and out-of-plane bending vibrations of *h*-BN,[33] respectively. In addition, the weaker band at 3398 cm^{-1} is related to N−H or O−H stretching vibrations or water molecules, widely observed in the BN system.[8,14] For **BU-110** and **BG-11** to **BG-115**, except for the previous main BN bands (772 and 1398 cm^{-1}), the spectra strongly differ from a previous report where dominant B−O bonds were observed and carbon was only present as an impurity.[14] Indeed, additional bands in our study due to carbon incorporation are assigned to C−N (1254 cm^{-1}), C═N (1632 cm^{-1}), and C≡N (2162 cm^{-1}). B−O bands (1200, 1350, 1450 cm^{-1}) are overlapping with the carbon−nitrogen bands. In agreement with XPS, FTIR demonstrates that carbon is involved in the structure of the as-obtained materials and is bonded to N to form a BCNO compound. In

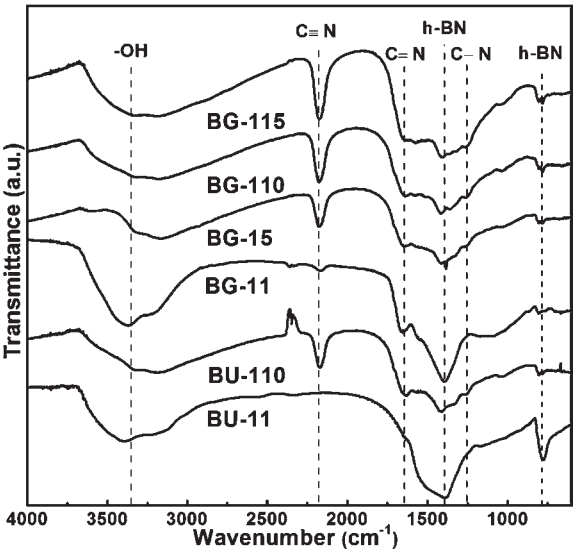

Figure 5. FTIR spectra of **BU-11**, **BU-110**, and **BG-11** to **BG-115**.

brief, structural characterizations by HRTEM, XRD, XPS, and FTIR suggest that the as-obtained samples are strongly related to layered *h*-BN when small amounts of C/N sources are used (**BU-11** and **BG-11**). On the other hand, BCNO samples are formed for higher C contents (**BG-15** to **BG-115**), where carbon is incorporated into the covalent framework of layered BN. B and C are then mostly bonded to the most electronegative element, that is, nitrogen, as previously observed.[8,14,34] Oxygen is incorporated into the material through B−O units because of the oxidation sensitivity of the less ordered surface sites. Although further

dx.doi.org/10.1021/ja200838c |*J. Am. Chem. Soc.* 2011, 133, 7121–7127

characterizations are certainly required to provide a better insight into the local structure of these BCNO, one might notice that the increase of the carbon content is correlated to the decrease of the interlayer distance measured by XRD, which becomes even smaller (0.327 nm for **BG-115**) than the values for *h*-BN (0.333 nm) and graphite (0.334 nm). It should also be noted that the presence of nanoscale carbon domains usually leads to black composites.[8] The colorful powders obtained herein are therefore an additional hint for the atomic scale incorporation of carbon and oxygen into the structure of the compounds, which strongly differs from previous studies.[8,14]

DLS was used to investigate the dispersion states in water. The hydrodynamic radii of **BU-110**, **BG-15**, **BG-110**, and **BG-115** are in the range 4−6 nm. These values agree with TEM pictures and show that the nanoparticles are dispersed in water (pH 6). Noteworthy, suspensions left to stand for 2 months did not show any visual sign of aggregation and yielded comparable DLS data. This underlines the excellent colloidal stability of these BCNO nanoparticles dispersions. Interestingly, increasing the temperature of synthesis at 800 °C yields lower solubility in water and precipitation of the solid from the suspension. This is ascribed to an increase of the particle size as shown by SEM (Figure S3), in agreement with the higher crystal order demonstrated by XRD (Figure S4). We investigated the surface state of the nanoparticles obtained at 700 °C by zeta potential measurements at different acidities. The values for **BG-110** and the corresponding hydrodynamic radii are shown in the Supporting Information (Figure S5). The nanoparticles are negatively charged with zeta potential values below −30 mV for pH ≥ 4. This corresponds to strongly negative surface charges, which account for colloidal stability. These charges most likely originate from B−O units, which are partially negatively charged as oxo or hydroxo groups. The zeta potential is less negative when the medium is acidified below pH 4. This corresponds to protonation of the oxo-hydroxo groups. Aggregation then occurs as demonstrated by the increase of the hydrodynamic radius. The behavior is, however, reversible, and aggregates can be readily broken by increasing the pH again. It is interesting to note that, although oxygen moieties are incorporated through a side reaction during washing in water, they are strongly beneficial to the colloidal properties of the material, providing stable aqueous dispersions over a wide pH range. A reference, blank test for a BCNO (**BG-110**) obtained without using any salt melt shows that the majority of the resulting sample is made of aggregates that precipitate. DLS measurements on the corresponding supernatant yield a bimodal size distribution with ca. 30 nm and 1 μm components. These sizes are much larger than those obtained for the molten salt-assisted process. The salt melt is therefore a suitable medium where the BCNO nanoparticles are stabilized during the synthesis and can be readily dispersed in water afterward. This contrasts with previous syntheses[13] without any solvent and exhibiting micrometer-size aggregates, which cannot be dispersed.

UV−visible absorption spectra were recorded to investigate the optical energy gap of the materials. As shown in Figure 6, both *h*-BN related samples **BU-11** and **BG-11** show an absorption edge at about 240 nm corresponding to a band gap energy of 5.2 eV, close to the value reported for *h*-BN.[6] The band gap of the other samples was roughly estimated to be 3.8−3.6 eV according to the onset of its spectrum, which is narrower than that of pure *h*-BN. This remarkable expansion to visible light region for all BCNO nanoparticles is mainly ascribed to carbon and oxygen incorporation into the structure of the compounds.[14−17]

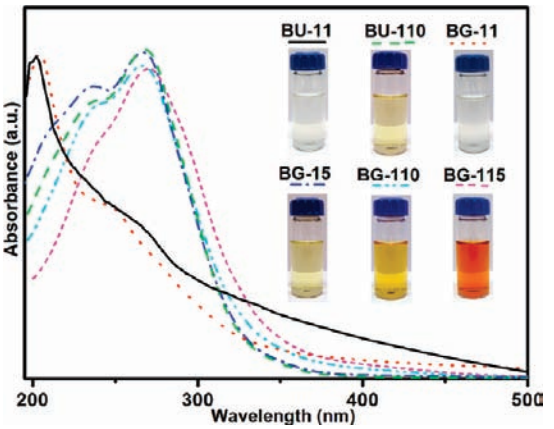

Figure 6. UV−visible absorption spectra of colloidal dispersions of **BU-11** and **BG-11**, **BU-110**, **BG-15**, **BG-110**, and **BG-115**. The insets are the corresponding digital pictures.

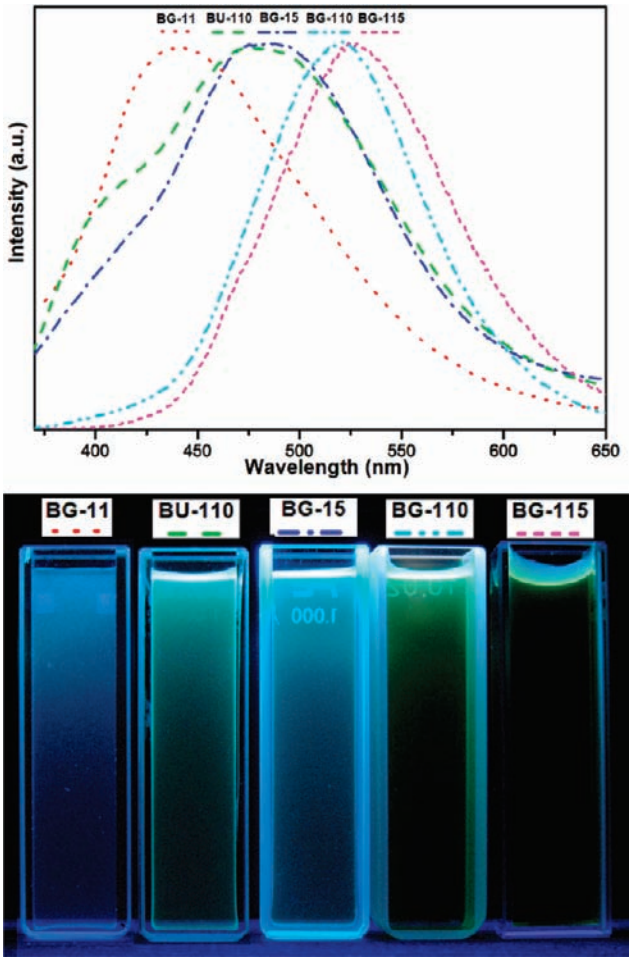

Figure 7. Emission spectra and digital photographs of colloidal dispersions of **BG-11**, **BU-110**, **BG-15**, **BG-110**, and **BG-115** with excitation light at 365 nm.

Figure 7 shows the photoluminescence (PL) spectra of the different colloidal dispersions with an excitation wavelength of 365 nm, chosen according to the excitation spectra for 475 nm emission (Figure S7), which are broad and cover a spectral region

from the UV to the visible regions. As pure *h*-BN, **BU-11** does not exhibit pholuminescence in the visible range and is not described in the figure. As for the absorption edge, the emission peak exhibits a red shift when the carbon content increases from **BG-11** (440 nm, blue emission) to **BU-110**, **BG-15**, **BG-110**, and **BG-115** (528 nm, green emission). Again, the spectral shifts may be attributed to carbon incorporation into the structure, which could reduce the band gap of BCNO compounds or induce defect-related energy levels.[14−16] In addition, the band gap of BCNO compounds has been reported to depend strongly on the atomic arrangement within the compounds.[13,14] This feature could also impact the optical properties of the material. The digital pictures (Figure 7) of the aqueous dispersions under 365 nm UV light further confirm that the emission wavelength is tunable. The efficiency of the fluorescence is reflected by the high absolute quantum yield (QY) measured by comparison with rhodamine B as reference.[35] We observed QY of 23%, 16%, 26%, 11%, and 5.6% for colloidal dispersions corresponding to **BU-110**, **BG-11**, **BG-15**, **BG-110**, and **BG-115**, respectively. These values seem to indicate that an increase of the carbon content leads to a decrease of the quantum yield, together with a red shift of the absorption. However, QY values as high as 26% are achieved without further specific optimization of the as-obtained materials. This value compares favorably to previous data obtained by a similar QY measurement technique for BCNO nanoparticles.[14] Noteworthy, reaching such high values for typical quantum dots in water usually requires coating with an inorganic and/or a ligand shell.[36,37] This simple comparison exemplifies the strong potential of the process reported herein for the fabrication of water-soluble photoluminescent nanoparticles.[38]

To assess the applicability of the particles for imaging in biological samples, we tested their activity toward lipid membranes. For this purpose, giant unilamellar vesicles,[29] representing a biomimetic cell-size system, were incubated in a dispersion of **BG-15**. The vesicles were made of a lipid typical for the outer leaflet of the plasma membrane of mammalian cells. Our preliminary tests (see Supporting Information Figure S8) suggest that the particles do not disrupt the membrane but are rather benign to it. Thus, the particles could be used, for example, for tracking the transport in trafficking vesicles in the cell. Further functionalization of the particles could ensure specific binding to proteins, which presents a future direction of this work.

4. CONCLUSIONS

In summary, we developed a simple, high yield, solution process to fabricate layered *h*-BN nanosheets with a thickness of less than 10 nm, and BCNO nanoparticles with a diameter of ca. 5 nm at temperatures as low as 700 °C. The procedure relies on a salt melt, which enables working under rather mild conditions, that is, atmospheric pressure and relatively low temperature, when compared to other processes. The solvent is environmentally benign, can be washed with water, and leads to readily dispersed nanoparticles without any post-treatment. Tuning the composition, especially the carbon content, is easily performed by adjusting the reactant ratio and the nature of the N/C source, thus yielding a versatile synthesis tool, which enables one to control the properties, here exemplified by visible light emission characteristics with good quantum yield. The as-obtained photoluminescent BCNO nanoparticles are believed to exhibit lower toxicity than typical Cd- or Pb-based quantum dots and are stable against aggregation in water over a wide range of pH without further chemical modification. Together with their very small size, all of these characteristics are promising for implementation in diagnostics and in optoelectronics.

■ ASSOCIATED CONTENT

Supporting Information. SEM image of **BG-11** sample, SEM image and XRD pattern of a sample synthesized at 800 °C, AFM and TEM pictures of **BG-15** and **BG-110** samples, B1s, C1s, and N1s XPS spectra of samples **BU-110**, **BG-110**, and **BG-115**, excitation spectrum of a dispersion of **BG-15** sample, and confocal images of **BG-15** nanoparticles in the presence of giant unilamellar vesicles. This material is available free of charge via the Internet at http://pubs.acs.org.

■ AUTHOR INFORMATION

Corresponding Author
david.portehault@upmc.fr

■ ACKNOWLEDGMENT

We acknowledge the Max-Planck Society and the Max-Planck Society − CNRS Postdoctoral Program for Nanomaterials for funding, Dr. Carmen Serra (Servicio de Nanotecnología y Análisis de Superficies, Universidad de Vigo) for XPS measurements and interpretations, Patricia Beaunier (UPMC) for HRTEM, and Xin-Hao Li for fruitful discussions.

■ REFERENCES

(1) Novoselov, K. S.; Geim1, A. K.; Morozov, S. V.; Jiang, D.; Katsnelson, M. I.; Grigorieva, I. V.; Dubonos, S. V.; Firso, A. A. *Nature* **2005**, *438*, 197–200.
(2) Kim, K. S.; Zhao, Y.; Jang, H.; Lee, S. Y.; Kim, J. M.; Kim, K. S.; Ahn, J. H.; Kim, P.; Choi, J. Y.; Hong, B. H. *Nature* **2009**, *457*, 706–710.
(3) Kubota, Y.; Watanabe, K.; Tsuda, O.; Taniguchi, T. *Science* **2007**, *317*, 932–934.
(4) Watanabe, K.; Taniguchi, T.; Niiyama, T.; Miya, K.; Taniguchi, M. *Nat. Photonics* **2009**, *3*, 591–594.
(5) Zeng, H. B.; Zhi, C. Y.; Zhang, Z. H.; Wei, X. L.; Wang, X. B.; Guo, W. L.; Bando, Y.; Golberg, D. *Nano Lett.* **2010**, *10*, 5049–5055.
(6) Song, L.; Ci, L. J.; Lu, H.; Sorokin, P. B.; Jin, C. H.; Ni, J.; Kvashnin, A. G.; Kvashnin, D. G.; Lou, J.; Yakobson, B. I.; Ajayan, P. M. *Nano Lett.* **2010**, *10*, 3209–3215.
(7) Yu, J.; Chen, Y.; Elliman, R. G.; Petravic, M. *Adv. Mater.* **2006**, *18*, 2157–2160.
(8) Portehault, D.; Giordano, C.; Gervais, C.; Senkovska, I.; Kaskel, S.; Sanchez, C.; Antonietti, M. *Adv. Funct. Mater.* **2010**, *20*, 1827–1833.
(9) Kawaguchi, M. *Adv. Mater.* **1997**, *9*, 615–625.
(10) Wang, W. L.; Bai, X. D.; Liu, K. H.; Xu, Z.; Golberg, D.; Bando, Y.; Wang, E. G. *J. Am. Chem. Soc.* **2006**, *128*, 6530–6531.
(11) Yin, L. W.; Bando, Y.; Golberg, D.; Gloter, A.; Li, M. S.; Yuan, X. L.; Sekiguchi, T. *J. Am. Chem. Soc.* **2005**, *127*, 16354–16355.
(12) Blank, V. D.; Seepujak, A. E.; Polyakov, V.; Batov, D. V.; Kulnitskiy, B. A.; Parkhomenko, Y. N.; Skryleva, E. A.; Bangert, U.; Gutiérrez-Sosa, A.; Harvey, A. J. *Carbon* **2009**, *473*, 167–3174.
(13) Ogi, T.; Kaihatsu, Y.; Iskandar, F.; Wang, W.; Okuyama, K. *Adv. Mater.* **2008**, *20*, 3235–3238.
(14) Liu, X. F.; Ye, S.; Qiao, Y. B.; Dong, G. P.; Zhang, Q.; Qiu, J. R. *Chem. Commun.* **2009**, 4073–4075.
(15) Rubio, A.; Corkill, J. L.; Cohen, M. L. *Phys. Rev. B* **1994**, *49*, 5081–5084.
(16) Mazzoni, M. S. C.; Nunes, R. W.; Azevedo, S.; Chacham, H. *Phys. Rev. B* **2006**, *73*, 073108.

(17) Watanabe, M. O.; Itoh, S.; Sasaki, T.; Mizushima, K. *Phys. Rev. Lett.* **1996**, *77*, 187–189.
(18) Bai, X. D.; Wang, E. G.; Yu, J.; Yang, H. *Appl. Phys. Lett.* **2000**, *77*, 67–69.
(19) Lee, C. G.; Li, Q.; Kalb, W.; Liu, X.; Berger, H.; Carpick, R. W.; Hone, J. *Science* **2010**, *328*, 76–80.
(20) Zhi, C.; Bando, Y.; Tang, C.; Kuwahara, H.; Golberg, D. *Adv. Mater.* **2009**, *21*, 2889–2893.
(21) Jin, C.; Lin, F.; Suenaga, K.; Iijima, S. *Phys. Rev. Lett.* **2009**, *102*, 195505.
(22) Shi, Y. M.; Hamsen, C.; Jia, X. T.; Kim, K. K.; Reina, A.; Hofmann, M.; Hsu, A. L.; Zhang, K.; Li, H. N.; Juang, Z. Y.; Dresselhaus, M. S.; Li, L. J.; Kong, J. *Nano Lett.* **2010**, *10*, 4134–4139.
(23) Nag, A.; Raidongia, K.; Hembram, K. P. S. S.; Datta, R.; Waghmare, U. V.; Rao, C. N. R. *ACS Nano* **2010**, *4*, 539–1544.
(24) Stéphan, O.; Ajayan, P. M.; Colliex, C.; Redlich, P.; Lambert, J. M.; Bernier, P.; Lefin, P. *Science* **1994**, *266*, 1683–1685.
(25) Zhang, Y.; Gu, H.; Suenaga, K.; Iijima, S. *Chem. Phys. Lett.* **1997**, *279*, 264–269.
(26) CI, L. J.; Song, L.; Jin, C. H.; Jariwala, D.; Wu, D. X.; Li, Y. J.; Srivastava, A.; Wang, Z. F.; Storr, K.; Balicas, L.; Liu, F.; Ajayan, P. M. *Nat. Mater.* **2010**, *9*, 430–435.
(27) Raidongia, K.; Nag, A.; Hembram, K. P. S. S.; Waghmare, U. V.; Datta, R.; Rao, C. N. R. *Chem.-Eur. J.* **2010**, *16*, 149–157.
(28) Briggs, D.; Seah, M. P. *Practical Surface Analysis*; Wiley: New York, 1990; Vol. 1.
(29) Dimova, R.; Aranda, S.; Bezlyepkina, N.; Nikolov, V.; Riske, K. A.; Lipowsky, R. *J. Phys.: Condens. Matter* **2006**, *18*, S1151–S1176.
(30) Xu, L. Q.; Peng, Y. Y.; Meng, Z. Y.; Yu, W. C.; Zhang, S. Y.; Liu, X. M.; Qian, Y. T. *Chem. Mater.* **2003**, *15*, 2675–2680.
(31) Bojdys, M. J.; Müller, J.-O.; Antonietti, M.; Thomas, A. *Chem.-Eur. J.* **2008**, *14*, 8177–8182.
(32) Thomas, A.; Fischer, A.; Goettmann, F.; Antonietti, M.; Müller, J. O.; Schlögl, R.; Carlsson, J. M. *J. Mater. Chem.* **2008**, *18*, 4893–4908.
(33) Geick, R.; Perry, C. H.; Rupprecht, G. *Phys. Rev.* **1966**, *146*, 543–547.
(34) Komatsu, T.; Goto, A. *J. Mater. Chem.* **2002**, *12*, 1288–1293.
(35) Demasa, J. N.; Crosby, G. A. *J. Phys. Chem.* **1971**, *75*, 991–1024.
(36) Peng, X.; Schlamp, M. C.; Kadavanich, A. V.; Alivisatos, A. P. *J. Am. Chem. Soc.* **1997**, *119*, 7019–7029.
(37) Han, H.-S.; Devaraj, N. K.; Lee, J.; Hilderbrand, S. A.; Weissleder, R.; Bawendi, M. G. *J. Am. Chem. Soc.* **2010**, *132*, 7838–7839.
(38) Zeng, H.; Duan, G.; Li, Y.; Yang, S.; Xu, X.; Cai, W. *Adv. Funct. Mater.* **2010**, *20*, 561–572.